Journal of Ceramic Processing Research. Vol. 13, No. 2, pp. 00~00 (2013)

J O U R N A L O F
Ceramic Processing Research

Effects of pressure and substrate positions on ZnO nanostructures during thermal evaporation of Zn Metal

Sin Young Bang[a], Tran Van Khai[a], Dong Keun Oh[a], Prachuporn Maneeratanasarn[a], Bong Geun Choi[a], Heon Ham[b], and Kwang Bo Shim[a,*]

[a]*Division of Materials Science and Engineering, Hanyang University, 17 Haengdang-dong, Seongdong-ku, Seoul 133-791, South Korea*

[b]*H&H Co. Ltd, Korea National University of Transportation, 50 Daehak-ro, Chungju-si, Chungbuk, 330-702, Korea*

ZnO nanostructures were prepared using a Zn metal source by the thermal evaporation process. The shapes of the ZnO nanostructures were changed depending on pressures and distances from the metal source in a tube furnace. One-dimensional nanowires with high crystallinity and density at an ambient atmospheric pressure were formed, while three-dimensional hollow structures resulted at low pressure. The influence of the pressure and distance from the metal source were evaluated by the SEM, XRD and TEM. The defect emission peaks originated from the remaining Zn metal and oxygen partial pressure were investigated by a photoluminescence (PL) analysis. The relationship between the nanostructural change and different pressures (or remaining Zn metal) is also explained.

Introduction

The physical and chemical properties of ceramic materials can be changed through control of their shapes [1-4]. Among the numerous types of ceramics, a multi-functional ZnO material is very important as it has a wide direct energy band gap of 3.37 eV and a large exciton binding energy (about 60 meV) at room temperature [5]. ZnO also can be changed its charactristics depending on the shapes and therefore there has been increasingly in-depth research on the nanostructural shapes of ZnO; nanowires [6, 7], nanotubes [8], nanobelts [9], nanodisks [10], hollow-structures [11], and others. A number of methods have been used to synthesize nanowires (NW), including solid-vapor phase processes such as thermal evaporation [6, 7], metal-organic chemical vapor deposition [12], and aqueous processes such as the hydrothermal method [13, 14]. Growth of vertically well-aligned morphologies of ZnO NWs is very important in the transference of electrons and photons. These properties offer many advantages for the assembly of optical/photonic devices. For the direct application of ZnO NWs to the direct devices, their size, density, and morphology are critical [15, 16]. ZnO hollow structures (HSs) with a large surface-to-volume ratio have attracted much attention due to their potential applications in catalysis, filler drug delivery, gas sensors, and photonics [17-22]. These ZnO HSs are classified into different shapes such as sphere [23], tube [24], cage [11] or cup [25]. They are typically synthesized by the template-dependent hydrothermal method [25, 26] and the thermal evaporation process [11, 23, 24, 27]. The former method is a complicated synthetic procedure and is difficult to fabricate various ZnO-HSs morphologies. However, the latter process is relatively easy and effective for the synthesis of ZnO-HSs with various morphologies.

This work presents the successful preparation of the realized NWs and HSs structures of ZnO using Zn metal by the thermal evaporation process. Through the catalyst-free process, pure products without impurities were also obtained. The effect of the ZnO HSs formation induced by the remaining Zn on the optical characteristics was evaluated. In particular, one-dimensional (NWs) and three-dimensional (tube, cage) morphologies were grown by controlling the internal pressure and distance between the metal source and the substrate during the growth process. The related mechanism for the shape changes of ZnO nanostructures (NSs) depending on the growing conditions are discussed and the experimental factors causing the change in their crystallinity and optical properties are also investigated presented.

Experimental

ZnO-NSs were synthesized by the thermal evaporation method. A schematic diagram of thermal evaporation system was illustrated in Fig. 1. The experimental system is a conventional horizontal electronic furnace

*Corresponding author:
Tel : +82-2220-0501
Fax: +82-2-2291-7395
E-mail: kbshim@hanyang.ac.kr (K.B.Shim)

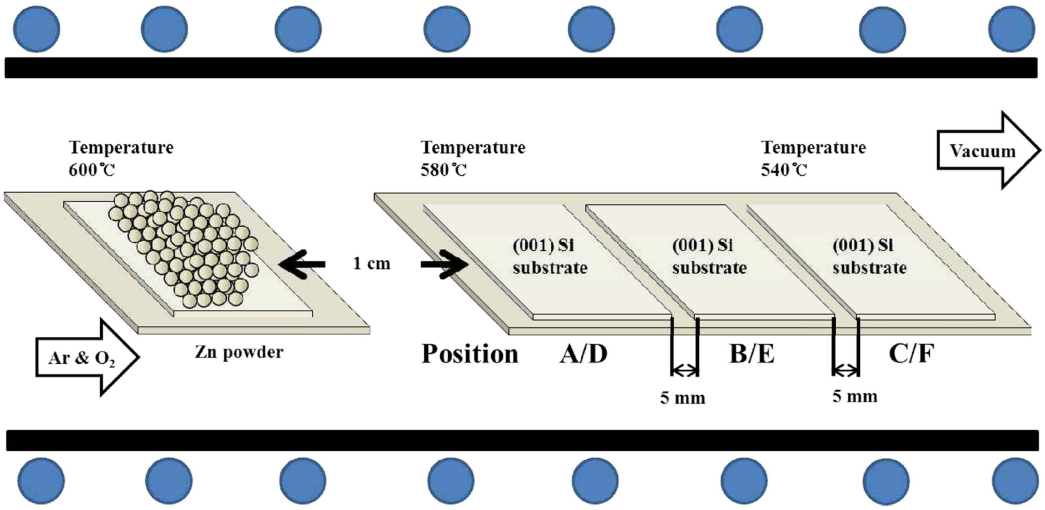

Fig. 1. A schematic diagram for the fabrication of ZnO nanostructures via thermal evaporation of the Zn metal.

using a quartz tube which is 1 inch in the inner diameter [28]. Si (100) wafers (1 × 1 cm) was used as the substrate for the synthesis of ZnO-NS. Before it uses substrate, the substrate was surface cleaning by pre-treatment. A 0.1 g pure metal the Zn powder (75 μm, 99.99%, Kojundo Chemical Lab. Japan) used as a Zn source and cleaned three substrates put in a prepared two alumina boats, respectively. The distance of a Zn source from substrateand between each substrate is 1 cm and 5 mm, respectively. After alumina boats being loaded into equipment, the pressure of a quartz tube was evacuated to 7.5 torr using a mechanical rotary pump. The growth experiment was progressed under atmosphericpressure and low partial pressure for observation of change morphologies of ZnO-NSs. In experiment process, after the purge process was complete, the pressure was increased to atmosphere again by Ar gas supply. After that, the reaction temperature was set 600 ºC and raised at a rate of 20 ºC/min. The growth process of ZnO-NWs was continued for 30 min. Ar and O_2 gas were introduced in to the system at 300 and 30 sccm by a mass flow controller (MFC), respectively. When the setting temperature of the Zn source was 600 ºC, the temperature of the section located inthe substrates was 580 ºC at position A and D, and 540 ºC at position C and F. After the experiment was over, the supply of all gases was interruptedand the quartz tube was cooled down to room temperature whileeach internal pressure was kept. The morphologies and the structural properties of the synthesized ZnO-NSs were characterized using scanning electron microscopy (SEM: JSM 5900 LV, JEOL, Japan), a high transmission electron microscope (TEM: JEOL, JEM-4010, 400 kV, Japan) and X-ray diffraction (XRD: Rigaku, Cu Kα wavelength at 1.53 Å, 40 kV, 30 mA, Japan). In addition, a photoluminescence (PL: KIMMON, IK-series, He-Cd laser, 325 nm, Japan) measurement was performed for the optical property.

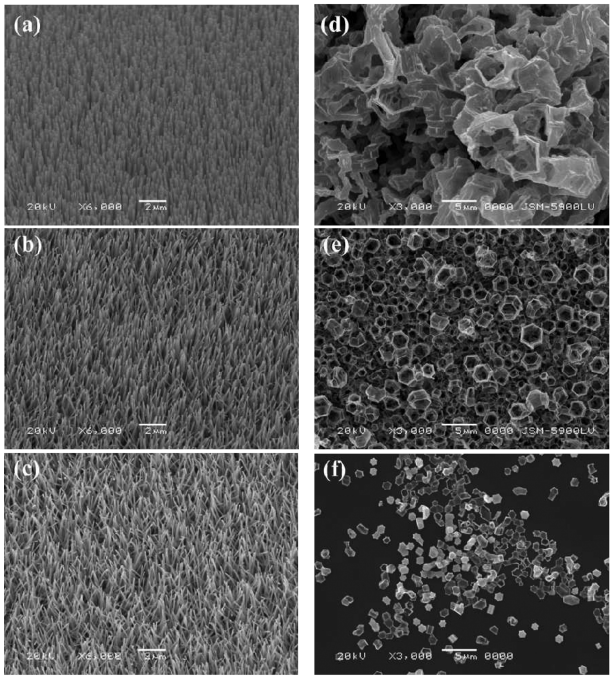

Fig. 2. SEM images of the grown ZnO nanostructures at different pressures and substrate positions. The images (a-c) represent tilted-view images of the ZnO nanowires grown at the position of 'A' to 'C' in atmospheric, while (d-f) shows the plane-view images of the ZnO hollow structures synthesized at positions 'D' to 'F' at low pressure, respectively.

Results and discussion

Fig. 2 shows the typical SEM images of ZnO-NSs grown as a function of the substrate position and at different pressure conditions (low and atmospheric). Fig. 2(a)-2(c) shows the morphologies of ZnO-NWs grown obtained at substrate positions 'A', 'B', and 'C', respectively, under atmospheric pressure. ZnO-NWs synthesized at position 'A'(Fig. 2(a)), which is a closed distance from the Zn source, indicate a growing

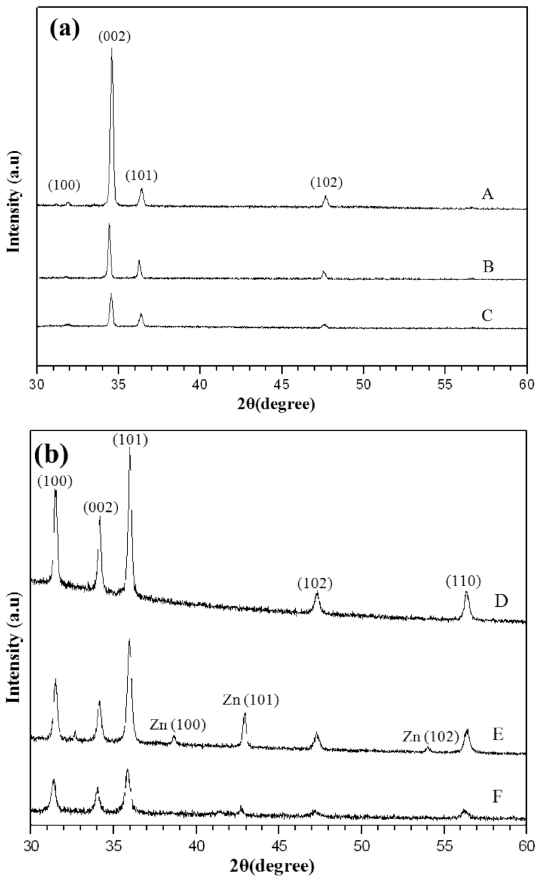

Fig. 3. XRD patterns of (a) ZnO nanowires grown at the position of 'A' to 'C' in the atmospheric pressure, and (b) ZnO hollow structures synthesized at the position of 'D' to 'F' in the low pressure, respectively.

tendency that is vertically well-aligned due to highly surface growth density. However, the products synthesized at position 'B'(Fig. 2(b)) and 'C'(Fig. 2(c)), which is a long distance from metal source, can be confirmed that a surface growth density and vertically alignment decrease. These results are known as complex factors such as crystallinity of initial formed ZnO layer, nucleation rate, concentration of metal source, distance form metal source, and growing temperature [28]. Fig. 2(d)-2(f) shows the morphologies of the ZnO-HSs synthesized at the substrate positions 'D', 'E', and 'F', respectively, under low pressure. The ZnO-HSs of polygonal winding tube type which lost its specific geometry was synthesized at position 'D' (see Fig. 2(d)). The average diameter of tube was 5 μm, and the shape was an irregular hexagonal structure. These shapes were due to the fact that the oxidation rate was much faster than evaporation rate of fused a Zn metal in HS by high concentration of a Zn source [27]. ZnO-HSs analogous to hexagonal cage shapes with an average diameter of 3 μm were synthesized at position 'E'(see Fig. 2(e)), and the frame of these cage structures consists of rod [11]. The ZnO hollow cage shapes with an average diameter of 1.5 μm were randomly observed on a substrate located at position 'F'(see Fig. 2(f)), and the typical shapes of the observed cage are classified into two groups: opened and closed cage types. The difference of nanostructure size/shape is assumed to be caused by distance of down stream, and self-assembly a Zn liquid droplets size, growing temperature, degree of surface oxidation reaction by oxygen concentration difference [11].

Fig. 3 shows the X-ray diffraction(XRD) pattern results of the ZnO-NS grown as a function of the substrate position and different pressure conditions (low and atmospheric). Fig. 3(a) shows the crystalline change of the ZnO-NSs grown at different substrate position under atmospheric pressure. As you can see from the graphic, grown ZnO-NWs are the wurtzite structure without intermediate or second-phases. The positions of the diffraction peaks of all the observed ZnO wurtzite structure are in good agreement with the standard ZnO (JCPDS No 05-0664). ZnO-NWs grown at the substrate position 'A', 'B', and 'C' revealed a high diffraction peak of (002) plan. These results indicate that the (002) plan of ZnO-NWs have vertical growth with a preferred orientation [29]. However, the diffraction peak intensity of the (002) plan decreased radically from 'A' to 'C' compared with diffraction intensity of the other diffraction plans such as (100), (101), and (102). As we confirmed in Fig. 2(a)-2(c), the vertical orientation and crystalline of the ZnO-NWs means decreased with increased distance from Zn metal source to substrate. Fig. 3(b) shows the crystalline change in the ZnO-NS grown at different substrate position under low pressure. The diffraction peaks of ZnO that indicate the wurtzite structure were all observed at the growing substrate position 'A', 'B', and 'C', but the strong preferred orientation characterization of (002) planas shown in Fig. 3(a) was not observed. The ZnO-NWs synthesized at position 'D', which is a closed distance form Zn source, only consisted of a single phase of ZnO. Even though the experiment was conducted at low pressure, position 'D' had a sufficient concentration of oxygen for formation of single ZnO phase. On the other hand, position 'E' and 'F' were found to have diffraction peaks which indicate non-oxidized Zn metal phases [11, 17]. These results were indicated that a remained Zn which does not vaporize in the interiors was not completely formed ZnO crystal by the lack oxygen concentration of surrounding during the ZnO-HS formation process. This result signified that the amount of the initially supplied oxygen was enough to form a single ZnO phase at position 'D', but not enough at position 'E' or 'F' because of the gradual consumption.

Fig. 4 shows a TEM analysis of the ZnO-NSs with NWs and HSs at the positions 'B' and 'E'. The low magnification TEM image shows the as-grown ZnO-NWs (position B) arrays in Fig. 4(a). The as-grown ZnO-NWs were found to have a straight shape with a diameter range of about 120 ~ 250 nm. No catalyst

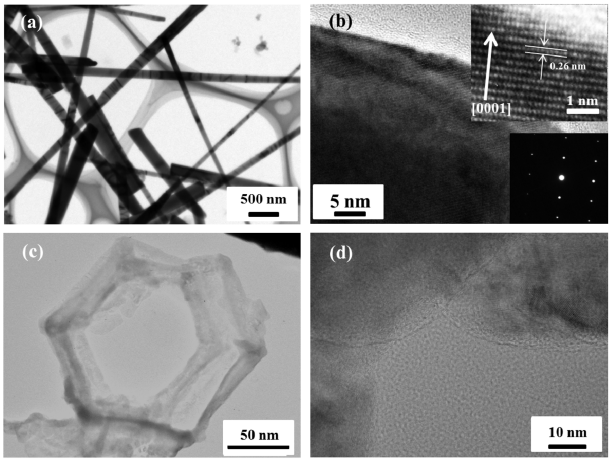

Fig. 4. TEM images show the growth of ZnO nanostructures at different pressures, (a) as-grown ZnO nanowires and (b) ZnO lattices, and the SAED pattern of the (0002) plane and the growth [0001] direction at position 'B', (c) the ZnO hollow structures and (d) the hexagonal edge of the three rods created at position 'E'.

particles could be observed at the top or bottom of the wires. This indicates that the growth of the ZnO-NWs is governed by a self-seeding vapor-solid (VS) mechanism. Fig. 4(b) shows a HR-TEM image of a single crystal ZnO-NWs. ZnO-NWs were found to have a clean surface without defects such as dislocations or stacking faults, oran amorphous layer on the surface. The HR-TEM image revealed no contamination and high crystalline quality. The inset in Fig. 4(b) displays the selected-area electron diffraction (SAED) pattern shows a single-crystal wurtzite structure with a c-axis orientation. The other inset in Fig. 4(b) is the lattice image of a single ZnO-NW. The lattice spacing of the as-grown ZnO-NW is about 0.26 nm between adjacent lattice planes corresponding to the distance between the (0002) crystal planes. The as-grown ZnO-NWs show highly preferential growth along the [0001] direction. These results indicate that the obtained ZnO-NWs are structurally homogeneous and defect free. The low magnification TEM image shows the ZnO-HSs (position E) in Fig. 4(c). The synthesized ZnO-HS has hollow hexagonal cage shape with shape size of 200 nm. The product edges are composed of the hexagon-based rods with a top and bottom surface. The ZnO-HSs is synthesized so that only the zinc metal powder without any metal catalyst were used to grow these structures, and those are made structure by self-assembly. The ZnO structure has crystallographic nature with different surfaces energies so that the low surface energy can be open the {0001} planes in the hollow structure [11]. Fig. 4(d) shows a HR-TEM image of top ZnO-HS edge. The edge is fabricated in a triangular shape form there single crystal rods. It is found that the composed rods have aclean surface, contains no defects, and have no amorphous layer on the surface or triangular connection.

Fig. 5 shows the schematic diagrams that explain the formation process of different NSs when the pressure in the quartz tube is at atmospheric and low. At the atmospheric pressure condition shown in Fig. 5(a), a vaporizable Zn of completely reacted oxygen was formed ZnO clusters, and these clusters were carried to the positions 'A', 'B' and 'C' by the carrier gas, which then it was formed ZnO layer [30-31]. ZnO layer have a high crystalline and c-axis orientation when the concentration of oxygen and temperature is increased. Also, the formation of ZnO layer is easy to vertical orientation growth of ZnO-NWs because the crystalline nuclear are easily formed [30-31], so that, as you can be seen from Fig. 2(a)-2(c), ZnO-NWs, which have high surface growth density, crystal size, crystal length,

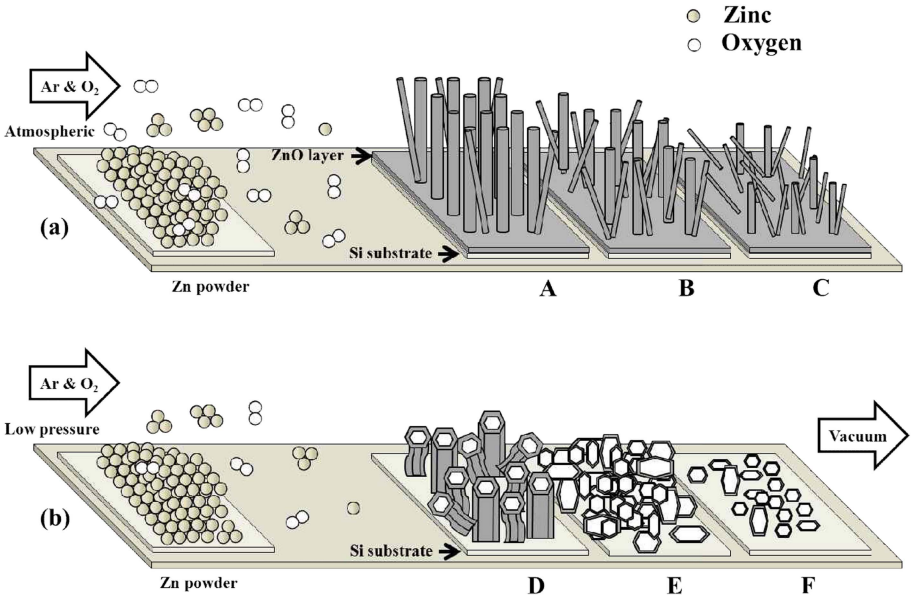

Fig. 5. Schematic diagrams representing the growth process for (a) ZnO nanowires and (b) hollow structures at oxygen partial pressure and different substrate positions.

vertical orientation growth, and crystalline [31-34] were grown at position 'A' rather than position 'C'. For low pressure condition, as shown in Fig. 5(b), a vaporizable Zn was not oxidized into ZnO due to the low concentration of oxygen and formed Zn clusters [11]. If the ratio of [Zn] : [O] is not close to 1 : 1, then this phenomenon is caused by existing Zn metal phase rather than the ZnO. The Zn clusters formfused Zn liquid droplets by self-assembly, in each other during carried on position by the Ar gas. And then the fused Zn liquid droplets are dropped on Si substrate in positions 'D', 'E', and 'F'. From these results, the fused Zn liquid droplets condense forming not non-spherical type but the hexagonal type on the substrateat relatively lower temperature, and then, it form the ZnO with a hexagonal type by surface oxidation [11]. The residual Zn in the forming ZnO plays a role for the stop reaction with oxygen [27]. Zn (T_m 419 °C) in the ZnO-HS was kept molten state by high substrate temperature of ambient (the temperatures of position D(T_D) and position F(T_F) are 580 °C and 540 °C, respectively) [35], so Zn was vaporized out between ZnO structure of surface [27, 36]. At this point, the (0002) face with the lowest energy collapsed, resulting in the formation of an open cage shape [11, 30]. Also, top and bottom surface of hexagonal-hollow structure (HS) are possible to grow of tube shape with (0002) crystal plane [11, 27]. Therefore, the internally vaporized ZnO forms a spherical or hexagonal-HS [11, 23, 24]. Thus, it is the large size, high crystalline, and high density of formed ZnO-HS at the position 'D', which has a high oxygen concentration and temperature, among the substrate positions ('D', 'E', and 'F'). These results can be confirmed from Fig. 2(d)-2(f). However, some Zn during this process were not completely oxidation but remained in interiors. This existence of Zn metal can confirm from XRD data in Fig. 3(b).

Fig. 6 shows the PL spectra analysis results of the optical properties for ZnO-NWs and ZnO-HS crystals grown by thermal evaporation processing. Fig. 5(a) shows the PL result of ZnO-NWs, demonstrating a strong intensity peak in 380 nm region. The surface growth density, c-axis orientation growth, and crystallinity of ZnO, known as a non-stoichiometric material, were increased at a closed 1 : 1 ratio of [Zn] : [O] and it was shown stronger luminescence property in 380 nm region [37-40]. Also, the [Zn]/[O] ratio is a non-stoichiometric, the donor/acceptor levels form by vacancies, interstitials, and antisite, and it increase the intensity in the visible region [40-43]. As shown in Fig. 6(a), the reason for the much stronger intensity of the PL spectrum at 380 nm of position 'A' was construed as a high surface growth density and the c-axis orientation. And the PL intensity of the ZnO grown at all position showed a lower intensity in 450 - 600 nm regions, which contributed to the defect of ZnO. The PL intensity of the position 'A' where there is a close

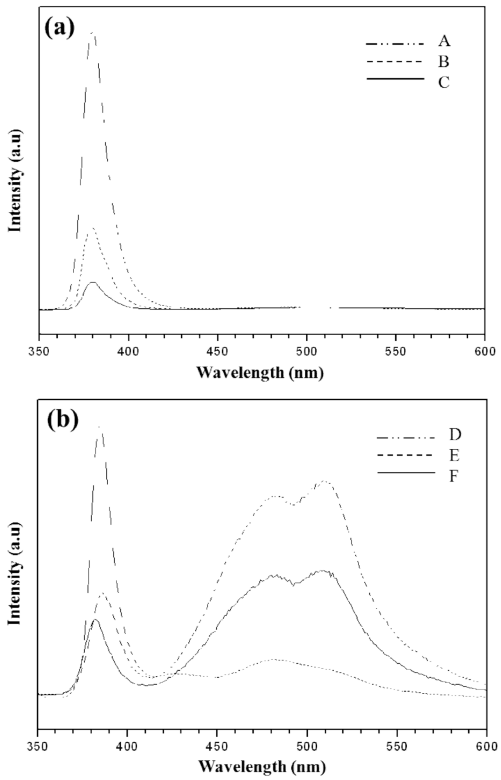

Fig. 6. Photoluminescence spectra of (a) ZnO nanowires and (b) the hollow structures at different substrate positions at the same oxygen partial pressure.

distance from the source is much stronger, and the PL intensity decrease with increasing distance from the source. We did not find evidence of formation of a donor/acceptor level. These were agreeing with results of SEM and XRD that ZnO was almost completely formed under atmospheric. And then the ZnO-NWs with high crystalline were grown as close distance from metal source, as well as the quality was decreased with increased distance from metal source. Fig. 6(b) shows the PL results of ZnO-HSs. The reason for the decreasein the PL intensity with increased distance from the Zn source metal was considered to be different of crystal various and growth density, as can be seen from Fig. 2(b) and Fig, 3(b). Also, each ZnO-HS were shown a very stronger luminescence characteristic in the visible region. It is generally the PL characteristic of ZnO, the region of 480 nm is related to intrinsic defects (O and Zn vacancies or interstitials in ZnO nanowires),and the region of 512 nm is related to singly ionized oxygen vacancy (V'_O, V''_O) centerby oxygen vacancy. The region of 590 nm is related to oxygen antisite state by excess oxygen. The region of 630 nm is related to the phenomenon of Zn deficiencies caused by the zinc vacancy (V_{Zn}) [40-43]. Therefore, the each PL region of ZnO-HS was caused by the intrinsic defects. This was the characteristic spectrum by interstitial Zn caused by the high concentration of Zn and oxygen vacancy by low oxygen partial pressure during growth

process. The reason the luminescence characteristics appearmuch stronger at the positions'E' and 'F' rather than position "D" may be due to the increase of defect concentration as the Zn/O ratio's non-stoichiometry was caused by low concentration of oxygen.

Conclusions

It was confirmed that ZnO-NSs with one-dimensional and three-dimensional structures were grown by oxygen partial pressure and the distance from metal source by the thermal evaporation process of Zn metal. The ZnO one-dimensional nanowires were grown when the oxygen partial pressure was atmospheric pressure, and we verified that it decreased growth density, vertical orientation, length of crystal, diameter of crystal, and PL intensity with increased distance from the metal source. On the other hand, the three-dimensional hollow structures, such as the tube and cage were grown at low oxygen partial pressure. It was decreased size, density, and increases distance from metal source, as well as it was confirmed that the intensity of luminescence was increased caused by defect in visual region. Therefore, in this study, we verified that the oxygen partial pressure plays an important role in the shape determination of ZnO-NSs during the thermal evaporation process. These results was considered that it have a potential application in efficiency improvement of electro-optics device through using ZnO-NSs.

References

1. A.P. Alivisatos, Science. 271 (1996) 933-937.
2. Y. Xia, P. Yang, Y. Sun, Y. Wu, B. Mayers, B. Gates, Y. Yin, F. Kim, and H. Yan, Adv. Mater. 15 (2003) 353-389.
3. J. Zhang, L. Sun, J. Yin, H. Su, C. Liao, and C. Yan, Chem. Mater. 14 (2002) 4172-4177.
4. J. Geng, D. Lu, J. Zhu, and H. Chen, J. Phys. Chem. B. 110 (2006) 13777-13785.
5. D.M. Bagnall, Y.F. Chen, Z. Zhu, T. Yao, S. Koyama, M.Y. Shen, and T. Goto, Appl. Phys. Lett. 70 (1997) 2230-2232.
6. M.H. Huang, Y. Wu, H. Feick, N. Tran, E. Weber, and P. Yang, Adv. Mater. 13 (2001) 113-116.
7. Z.L. Wang, J. Phys. Condens. Matter. 16 (2004) R829-R858.
8. J.J. Wu, S.C. Liu, T.C. Wu, K.H. Chen, and L.C. Chen, Appl. Phys. Lett. 81 (2002) 1312-1314.
9. Y.J. Xing, Z.H. Xi, Z.Q. Xue, X.D. Zhang, J.H. Song, R.M. Wang, J. Xu, Y. Song, S.L. Zhang, and D.P. Yu, Appl. Phys. Lett. 83 (2003) 1689-1691.
10. X.L. Zhang, R. Qiao, R. Qiu, J.C. Kim, and Y.S. Kang, Cryst. Growth & Design. 9 (2009) 2906-2910.
11. P.X. Gao, and Z.L. Wang, J. Am. Chem. Soc. 125 (2003) 11299-11305.
12. B.P. Zhang, N.T. Binh, K. Wakatsuki, Y. Segawa, Y. Yamada, N. Usami, M. Kawasaki, and H. Koinuma, Appl. Phys. Lett. 84 (2004) 4098-4100.
13. M. Law, L.E. Greene, J.C. Jhonson, R. Saykallya, and P. Yang, Nat. Mater. 4 (2005) 455-459.
14. B.G. Wang, E.W. Shi, and W.Z. Zhong, Cryst. Res. Technol. 33 (1998) 929-935.
15. S.H. Jo, J.Y. Lao, Z.F. Ren, R.A. Farrer, T. Baldacchini, and J.T. Fourkas, Appl. Phys. Lett. 83 (2003) 4821-4823.
16. Y.W. Zhu, H.Z. Zhang, X.C. Sun, S.Q. Feng, J. Xu, Q. Zhao, B. Xiang, and R.M. Wang, Appl. Phys. Lett. 83 (2003) 144-146.
17. A. Umar, S.H. Kim, Y.H. Im, and Y.B. Hahn, Superlattices Microstruct. 39 (2006) 238-246.
18. H.P. Liang, H.M. Zhang, J.S. Hu, Y.G. Guo, L.J. Wan, and C.L. Bai, Angew. Chem. Int. Ed. 43 (2004) 1540-1543.
19. M. Ohmori, and E. Matijevic, J. Colloid Interface Sci. 150 (1992) 594-597.
20. E. Mathiowitz, J.S. Jacob, Y.S. Jong, G.P. Carino, D.E. Chickering, P. Chaturvedi, C.A. Santos, K. Vijayaraghavan, S. Montgomery, M. Bassett, and C. Morrell, Nature 386 (1997) 410-414.
21. Z. Miao, Y. Wu, X. Zhang, Z. Liu, B. Han, K. Ding, and G. An, J. Mater. Chem. 17 (2007) 1791-1796.
22. J.C. Johnson, H. Yan, P. Yang, and R.J. Saykally, J. Phys. Chem. B. 107 (2003) 8816-8828.
23. D.H. Fan, Appl. Phys. A. 96 (2009) 655-660.
24. S.L. Mensah, V.K. Kayastha, I.N. Ivanov, D.B. Geohegan, and Y.K. Yap, Appl. Phys. Lett. 90 (2007) 113108.
25. S.H. Jung, E.G. Oh, K.H. Lee, Y.S. Yang, C.G. Park, W.J. Park, and S.H. Jeong, Cryst. Growth & Design. 8 (2008) 265-269.
26. G.R. Li, S.H. Lu, W.X. Zhao, C.Y. Su, and Y.X. Tong, Cryst. Growth & Design 8 (2008) 1276-1281.
27. J.Q. Hu, Q. Li, X.M. Meng, C.S. Lee, and S.T. Lee, Chem. Mater. 15 (2003) 305-308.
28. T.V. Khai, S.Y. Bang, D.K. Oh, B.G. Choi, and K.B. Shim, J. Ceramic Processing Research 12 (2011) 106-109.
29. N. Fufimura, T. Nishihara, S. Goto, J. Xu, and T. Ito, J. Crystal. Growth. 130 (1993) 269-279.
30. A. Umar, H.W. Ra, J.P. Jeong, E.K. Suh, and Y.B. Hahn, Korean J. Chem. Eng. 23 (2006) 499-504.
31. H.M. Cheng, H.C. Hsu, S. Yang, C.Y. Wu, Y.C. Lee, L.J. Lin, and W.F. Hsieh, Nanotechnology 16 (2005) 2882-2886.
32. S.Y. Li, P. Lin, C.Y. Lee, T.Y. Tseng, and C.J. Huang, J. Phys. D: Appl. Phys. 37 (2004) 2274-2282.
33. H.C. Hsu, C.S. Cheng, C.C. Cheng, S. Yang, C.S. Chang, and W.F. Hsieh, Nanochnology 16 (2005) 297-301.
34. U. Manzoor, and D.Y. Kim, Physica E. 41(2009) 500-505.
35. H.A. Wriedt, Bulletin of Alloy Phase Diagrams 8 (1987) 166-176.
36. J.J. Wu, S.C. Liu, C.T. Wu, K.H. Chen, and L.C. Chen, Appl. Phys. Lett. 81 (2002) 1312-1314.
37. K.H. Tam, C.K. Cheung, Y.H. Leung, A.B. Djurišic´, C.C. Ling, C.D. Beling, S. Fung, W.M. Kwok, W.K. Chan, D.L. Phillips, L. Ding, and W.K. Ge, J. Phys. Chem. B 110 (2006) 20865-20871.
38. H.J. Son, K.A. Jeon, C.E. Kim, J.H. Kim, K.H. Yoo, and S.Y. Lee, Appl. Surf. Sci. 253 (2007) 7848-7850.
39. K.A. Jeon, H.J. Son, C.E. Kim, J.H. Kim, and S.Y. Lee, Physica. E. 37 (2007) 222-225.
40. A. Chatterjee, C.H. Shen, A. Granguly, L.C. Chen, C.W. Hsu, J.Y. Hwang, and K.H. Chen, Chem. Phys. Lett. 391 (2004) 278-282.
41. M.L. Cui, X.M. Wu, L.J. Zhuge, and Y.D. Meng, Vacuum 81 (2007) 899-903.
42. A.B. Djurišic´, Y.H. Leung, K.H. Tam, Y.F. Hsu, L. Ding, W.K. Ge, Y.C. Zhong, K.S. Wong, W.K. Chan, H.L. Tam, K.W. Cheah, W.M. Kwok, and D.L. Phillips, Nanotechnology 18 (2007) 095702.
43. A. vanDijken, E.A. Meulenkamp, D. Vanmaekelbergh, and A. Meijerink, J. Phys. Chem. B. 104 (2000) 1715-1723.